Clinical and Experimental Obstetrics & Gynecology

Clin. Exp. Obstet. Gynecol. **2026**; 53(9): 53703
https://doi.org/10.31083/CEOG53703

Original Research

Preoperative Three-Dimensional Magnetic Resonance Angiography-Based Anatomical Risk Stratification in Transvaginal Sacrospinous Ligament Fixation: A Preliminary Predictive Analysis of Intraoperative Hemorrhage and Postoperative Complications

Chao Zhang[1], Yajuan Gao[2], Shuncang Zhang[3], Xiaochun Huang[1], Qing Su[1], Ji Yang[1], Huijuan Peng[1], Jianfeng Wang[1,*]

[1]Department of Obstetrics and Gynecology, Xi'an People's Hospital (Xi'an Fourth Hospital), 710004 Xi'an, Shaanxi, China
[2]Department of Radiology, Peking University Third Hospital, 100191 Beijing, China
[3]Department of Obstetrics and Gynecology, Xi'an Daxing Hospital, 710016 Xi'an, Shaanxi, China
*Correspondence: wangjf1106@163.com (Jianfeng Wang)

Academic Editor: Ugo Indraccolo
Submitted: 9 May 2026 Revised: 8 June 2026 Accepted: 24 July 2026 Published: 9 September 2026

Abstract

Background: To establish a preliminary three-tier anatomical risk classification for sacrospinous ligament fixation (SSLF) using preoperative three-dimensional (3D) magnetic resonance angiography (MRA), evaluate its correlation with intraoperative hemorrhage and postoperative complications, as well as compare perioperative outcomes between MRA-guided and conventional SSLF while accounting for potential confounding between risk stratification and tailored surgical approaches in the MRA cohort. **Methods:** This single-center, parallel-group randomized controlled trial was conducted at a tertiary gynecological center in China from January 2024 through December 2025. A total of 140 patients with pelvic organ prolapse quantification (POP-Q) stage III–IV uterine prolapse scheduled for uterus-preserving transvaginal SSLF were randomly assigned in a 1:1 ratio to either a 3D MRA-guided group (n = 70), which underwent preoperative MRA with 3D reconstruction and individualized surgical planning, or a conventional palpation-guided group (n = 70), which underwent standard tactile-guided surgery without preoperative MRA. In the MRA-guided group, bilateral sacrospinous ligament (SSL) morphometry and the spatial relationship with the internal pudendal artery (IPA) were quantified using 3D reconstructions (Mimics version 19.0). Patients were classified into three anatomical risk categories: Type I (standard risk: IPA distance ≥20 mm and thickness ≥3.5 mm), Type II (moderate risk: IPA distance 15–19 mm or thickness 2.5–3.4 mm), and Type III (high risk: IPA distance <15 mm or thickness <2.5 mm). Primary outcomes comprised operative time, estimated blood loss (EBL), and length of hospital stay. Prespecified secondary outcomes included 6-month overall postoperative complication rates and 1-month Pelvic Floor Distress Inventory-20 (PFDI-20) scores. Risk-stratified subgroup analyses, univariate receiver operating characteristic (ROC) curve analyses, and Cochran–Armitage trend testing were designated as post hoc exploratory analyses, with no formal adjustment for multiple comparisons applied. Multivariable logistic regression analysis was performed solely in the full study cohort; subgroup regression analysis within the MRA-guided group was omitted due to severe overfitting risk from limited complication events. **Results:** Baseline demographic characteristics demonstrated acceptable intergroup balance, with all standardized mean differences (SMDs) <0.2, except for BMI (SMD = 0.448) showing moderate imbalance; BMI was included as a covariate in multivariable regression to account for this imbalance, rather than relying on p-value comparisons to confirm randomization success. The MRA-guided group exhibited a significantly shorter operative time (56.2 ± 9.8 vs. 74.8 ± 11.6 min, $p < 0.001$), reduced median EBL (39 [32–51] vs. 64 [53–79] mL, $p < 0.001$), and shorter hospitalization (3.2 ± 0.5 vs. 4.5 ± 1.1 d, $p < 0.001$). Median EBL was reported alongside mean ± standard deviation (SD) to account for four extreme hemorrhage outliers (210, 225, 240, and 270 mL) in the conventional arm, which distorted the distribution of raw EBL values. The overall complication rates were significantly lower in the MRA-guided group than in the conventional group (7.1% [5/70] vs. 24.3% [17/70], χ^2 = 8.14, p = 0.004). Within the MRA-guided group, risk-type distribution was: Type I 44.3% (31/70), Type II 37.1% (26/70), and Type III 18.6% (13/70). Complication rates increased descriptively across risk types (3.2%, 7.7%, and 15.4% for Types I–III, respectively), although the Cochran–Armitage trend test did not reach statistical significance (p-value = 0.157). All four intraoperative vascular injuries occurred in the non-MRA group; no neurovascular injuries were observed in the MRA-guided cohort. On multivariable logistic regression including all 140 patients, assignment to the non-MRA group emerged as an independent predictor of postoperative complications (adjusted odds ratio [OR] = 4.1; 95% confidence interval [CI]: 1.3–12.8, p = 0.015). Separate univariate ROC curve analyses were conducted in distinct study populations. Among all participants, binary group allocation yielded an area under the curve (AUC) of 0.66 (95% CI: 0.57–0.75); within the MRA cohort, the three-tier risk classification achieved an AUC of 0.67 (95% CI: 0.54–0.80), outperforming IPA distance alone (AUC = 0.63; 95% CI: 0.50–0.76) and SSL thickness alone (AUC = 0.60; 95% CI: 0.47–0.73). A combined predictive model integrating group assignment and MRA risk type was excluded from analysis, as anatomical risk stratification data were unavailable for all patients in the conventional arm, thereby precluding construction of a unified model. Direct DeLong comparisons between ROC curves derived from non-overlapping patient subsets were not performed in accordance with methodologic

guidance. **Conclusions:** The 3D MRA-derived SSL–pudendal vascular risk classification provides a preliminary framework for preoperative anatomical stratification in patients undergoing SSLF, with incremental descriptive associations with intraoperative hemorrhage and postoperative adverse events. Type III anatomical features were associated with a numerically higher complication risk despite the use of image-adapted surgical technique. **Clinical Trial Registration:** The trial was registered with the Chinese Clinical Trial Registry (ChiCTR) at https://www.chictr.org.cn (registration number ChiCTR2600121272).

Keywords: uterine prolapse; sacrospinous ligament fixation; magnetic resonance angiography; 3D reconstruction; image-guided surgery; pelvic organ prolapse

1. Introduction

Pelvic organ prolapse (POP) constitutes one of the most prevalent pelvic floor disorders affecting women in later life, with estimated lifetime surgical risk ranging from 11% to 19% [1]. Among the reconstructive procedures currently available, transvaginal sacrospinous ligament fixation (SSLF) has been widely adopted as a native tissue, mesh-sparing technique for apical prolapse repair as it provides vaginal access, relatively low procedural cost, and preservation of vaginal length [2]. Nevertheless, the clinical efficacy of SSLF depends critically upon accurate suture placement within the sacrospinous ligament (SSL), which lies in intimate proximity to the internal pudendal artery (IPA), inferior gluteal artery, and sciatic nerve [3]. Anatomical studies have revealed substantial interindividual variability in the spatial relationships between these neurovascular structures and the ligament, with the IPA-to-SSL distance ranging from as little as 8 mm to over 25 mm among individuals [4,5].

Conventional SSLF relies exclusively on the surgeon's tactile perception to localize the ligament and estimate suture depth, an inherently subjective approach that affords no preoperative awareness of vascular proximity [6]. Consequently, vascular injury during SSLF, most commonly involving branches of the IPA, has been documented in 3% to 8% of cases, and severe hemorrhage requiring transfusion or embolization occurs in a clinically meaningful subset of patients [7,8]. The inability to pre-identify patients harboring elevated anatomical risk preoperatively remains a critical and longstanding gap in the current surgical planning for SSLF.

Three-dimensional (3D) reconstruction based on magnetic resonance angiography (MRA) has emerged as a powerful modality for preoperative anatomical mapping across diverse surgical specialties, including living donor nephrectomy, orthopedic ligament reconstruction, and hepatic resection [9,10,11]. In the context of pelvic floor surgery, 3D MRA enables precise quantification of SSL dimensions and their spatial relationships with adjacent vasculature, thereby potentially transforming surgical planning from an experience-based paradigm to a data-driven, individualized approach [12,13]. However, prior studies have described primarily the feasibility of 3D reconstruction without establishing a systematic classification framework linking anatomical measurements to surgical risk. Notably, the existing anatomical literature has not distinguished baseline vascular risk from surgical technique modifications introduced when imaging data inform intraoperative decision-making, a critical confounding factor that is addressed within the limitations of the present study.

We hypothesized that specific MRA-derived anatomical parameters, particularly the IPA-to-SSL distance and SSL thickness, could be integrated into a risk stratification system that is descriptively associated with intraoperative hemorrhage and postoperative complications. Furthermore, we hypothesized that 3D MRA-guided surgical planning would reduce overall complication rates compared with conventional palpation-guided surgery performed without preoperative imaging. Accordingly, the present study pursued three objectives: (1) to develop a preliminary three-tier SSL–pudendal vascular risk classification based on preoperative 3D MRA measurements in patients undergoing MRA-guided SSLF; (2) to descriptively evaluate the correlation of this classification with intraoperative blood loss and 6-month postoperative complications within the MRA-guided group through post hoc exploratory analyses; and (3) to determine whether 3D MRA-guided planning reduces overall adverse outcomes compared with conventional palpation-guided SSLF without preoperative imaging using prespecified primary and secondary endpoints.

2. Materials and Methods

2.1 Study Design and Ethical Considerations

This single-center, parallel-group randomized trial was conducted at the Department of Obstetrics and Gynecology, Xi'an People's Hospital, a tertiary gynecological referral center in China. Patients were enrolled between January 2024 and December 2025. The study was conducted in accordance with the Declaration of Helsinki and reported according to Consolidated Standards of Reporting Trials (CONSORT) guidelines for randomized trials. The study protocol was approved by the Institutional Ethics Committee of Xi'an People's Hospital (Approval No.: 20220117; approval date: January 17, 2022). Written informed consent was obtained from all participants before randomization. Consent for publication of the clinical image was obtained.

2.2 Sample Size Estimation

Sample size was calculated a priori using G*Power 3.1 software (Heinrich-Heine-Universität Düsseldorf, Germany) with dual statistical rationales to accommodate both primary endpoint analysis and post hoc subgroup risk stratification:

Primary endpoint calculation (operative time): Pilot cohort data (n = 24) demonstrated a large effect size (d = 1.76) for operative time between palpation-guided and 3D MRA-guided surgery. For a two-tailed independent-samples t-test ($\alpha = 0.05$, power = 0.80, allocation ratio 1:1), this effect size required a minimum of 8 patients per group to detect differences in operative time alone.

Secondary subgroup analysis adjustment: The prespecified exploratory objective of stratifying the MRA cohort into three distinct anatomical risk subgroups required a larger sample size to reduce the likelihood of underpowered descriptive comparisons. After accounting for an anticipated 15% dropout or exclusion rate applied to the minimum primary endpoint sample (46 patients per group to stabilize subgroup distribution), a target enrollment of 70 patients per group (total n = 140) was selected to ensure adequate representation within Type I, II, and III risk subsets for descriptive post hoc evaluation. A simple 15% inflation of the 46-patient minimum sample would yield 54 patients per group; the additional 16 patients per group were prospectively enrolled to safeguard statistical stability for risk-stratified exploratory analyses, as documented in the original institutional study protocol.

2.3 Participants

Inclusion criteria were as follows: (1) women aged 40–70 years; (2) confirmed pelvic organ prolapse quantification (POP-Q) stage III or IV on standardized gynecological examination; (3) planned uterus-preserving transvaginal SSLF; (4) ability to comply with the stipulated follow-up schedule; and (5) provision of written informed consent.

Exclusion criteria were as follows: (1) concurrent hysterectomy indicated for gynecologic malignancy or other benign uterine pathology [14]; (2) contraindications to MRI/MRA (e.g., ferromagnetic implants or severe claustrophobia), this criterion was applied to all potential participants, as patients with contraindications to MRI could not be randomized to the MRA-guided arm; (3) history of major pelvic surgery, including prior prolapse repair, radical hysterectomy, pelvic fracture fixation; (4) cognitive impairment precluding informed consent; (5) severe cardiopulmonary, hepatic, or renal disease rendering surgery unsafe; and (6) current pregnancy or lactation.

2.4 Randomization, Allocation Concealment, and Blinding

Eligible patients were randomly assigned in a 1:1 ratio to either the 3D MRA-guided group or the conventional non-MRA group using a computer-generated allocation sequence prepared by an independent biostatistician. Allocation concealment was maintained with sequentially numbered, sealed, opaque envelopes that were opened only after informed consent had been obtained. Blinding of the operating surgeon was not feasible because the intervention required preoperative imaging and individualized surgical planning modifications. Postoperative outcome assessors and the statistical analyst remained blinded to group assignment until database lock.

2.5 Interventions

2.5.1 3D MRA-Guided Group (n = 70)

MRA Acquisition: Patients assigned to the MRA-guided group underwent preoperative pelvic MRA on a 3.0-T scanner (SIGNA HDxt; GE Medical Systems, Waukesha, WI, USA) using standard pelvic imaging protocols. Gadobutrol (Gadavist; Bayer HealthCare, Berlin, Germany) was administered intravenously as the contrast agent. Raw DICOM data were archived for subsequent postprocessing.

3D Reconstruction and Anatomical Measurements: Two senior radiologists, blinded to surgical outcomes, independently imported MRA datasets into Mimics version 19.0 (Materialise NV, Leuven, Belgium) to construct 3D models of the pelvis, SSL, and adjacent neurovascular structures, including IPA, inferior gluteal artery, and sciatic nerve. The following parameters were measured bilaterally: (a) SSL thickness at the thickest point; (b) SSL width; (c) distance from the SSL to the IPA; (d) distance from the SSL to the inferior gluteal artery; (e) distance from the pudendal canal (Alcock's canal) to the ischial spine; and (f) distance from the thickest point of the coccygeus–SSL complex to the ischial spine. Interobserver agreement was quantified using intraclass correlation coefficients (ICCs).

Risk Classification: Based on the MRA measurements, each patient in the MRA-guided group was assigned an anatomical risk category according to prespecified thresholds derived from the pilot cohort and published anatomical data [5,15]:

Type I (Standard Risk): IPA-to-SSL distance ≥20 mm and SSL thickness ≥3.5 mm.

Type II (Moderate Risk): IPA-to-SSL distance 15–19 mm or SSL thickness 2.5–3.4 mm (without meeting Type III criteria).

Type III (High Risk): IPA-to-SSL distance <15 mm or SSL thickness <2.5 mm.

When bilateral measurements differed, classification was determined by the side with the smaller IPA-to-SSL distance or thinner ligament, in accordance with a worst-case-scenario principle designed to maximize patient safety.

Surgical Planning and Execution: Two senior gynecologists and the radiologists collaboratively reviewed the 3D models to develop individualized suture plans. The optimal suture corridor was defined as the region of maximal ligament thickness (≥3.0 mm) while maintaining ≥15 mm clearance from the IPA. For patients classified as Type

III, a multipoint shallow-suture technique (depth <2 mm, ≤2 sutures) was planned preoperatively to minimize vascular injury risk. The surgeon referred intraoperatively to a sterile-printed reference sheet displaying the 3D model, key anatomical measurements, and the planned suture corridor. This risk-adapted surgical modification introduces critical sources of confounding, as observed differences in complication rates across risk strata likely reflect both underlying anatomical vulnerability and modified intraoperative technique. These effects cannot be separated without a three-arm trial design (MRA measured unused, MRA guided, no MRA).

2.5.2 Conventional Palpation-Guided (Non-MRA) Group (n = 70)

Patients assigned to the conventional group did not undergo preoperative MRA examination. SSLF was performed according to the institutional standard tactile-guided technique, with suture placement determined solely by the surgeon's palpation of the SSL and adjacent anatomical landmarks. No imaging data or 3D models were available to the surgical team for this group. In addition, no standardized anatomical measurements were captured for patients in the conventional arm, precluding risk-stratified cross-group comparisons.

All procedures were performed by a single experienced pelvic floor surgeon (≥200 prior SSLF procedures) to eliminate intersurgeon variability. Absorbable sutures (Ethicon, Johnson & Johnson, Somerville, NJ, USA) and perioperative prophylactic cefazolin (CSPC Pharmaceutical, Shijiazhuang, Hebei, China) were used uniformly across both groups.

2.6 Follow-up Protocol

Postoperative follow-up was conducted at 1 week, 1 month, 3 months, and 6 months via outpatient visits and telephone contact. At each assessment, complications such as lower-limb neuropathy, urinary dysfunction, wound infection, prolapse recurrence, and vascular or nerve injury, were systematically recorded. Pelvic floor function was assessed at 1 month using the Pelvic Floor Distress Inventory-20 (PFDI-20) questionnaire, and anatomical outcomes were evaluated at 3 and 6 months by the POP-Q system. No patients were lost to follow-up during the 6-month observation period.

2.7 Outcome Measures

Prespecified Primary Outcomes: (1) operative time, defined as the interval from vaginal incision to completion of suturing; (2) estimated blood loss (EBL), calculated from suction volume + gauze weighing, and reported as both mean ± standard deviation (SD) and median (interquartile range, IQR) to account for non-normal distribution and hemorrhage outliers; and (3) postoperative hospital stay, defined as the interval from the date of surgery to discharge-criteria fulfillment.

Prespecified Secondary Outcomes: (1) incidence of any postoperative complication within 6 months; (2) PFDI-20 score at 1 month; and (3) POP-Q stage at 3 and 6 months.

Post Hoc Exploratory Outcomes (Not Registered in the Trial Protocol): (1) within the MRA-guided group, risk-type-stratified descriptive analyses of EBL, operative time, PFDI-20 score, and complication rates; (2) univariate receiver operating characteristic (ROC) curve analyses to assess discriminative performance of binary group allocation, IPA distance, SSL thickness, and the three-tier risk classification, analyzed in separate non-overlapping patient populations; and (3) multivariable logistic regression restricted to the full 140-patient cohort to identify independent predictors of postoperative complications. Multivariable regression within the MRA subgroup was excluded due to extreme event-per-variable imbalance and overfitting risk.

2.8 Statistical Analysis

All analyses were performed in the intention-to-treat (ITT) population using IBM SPSS Statistics version 27.0 (IBM Corp., Armonk, NY, USA) and MedCalc version 20.0 (MedCalc Software, Ostend, Belgium). Continuous variables were assessed for normality (Shapiro–Wilk test) and variance homogeneity (Levene's test). Normally distributed data were expressed as mean ± SD and compared via independent-samples *t*-tests. Non-normally distributed variables (including EBL) were supplemented with median (IQR), and between-group comparisons were conducted via Mann–Whitney U tests. Categorical variables were presented as counts (percentages) and compared using chi-square tests (with Fisher's exact test when expected cell counts were <5). Baseline intergroup balance was quantified using standardized mean differences (SMDs), and reliance on *p*-values to confirm randomization success was avoided in accordance with CONSORT recommendations. Cochran–Armitage trend testing was applied to evaluate linear trends in complication rates, EBL, operative time, and PFDI-20 scores across MRA risk subtypes. All trend analyses were classified as post hoc exploratory assessments without formal multiplicity adjustment.

Multivariable logistic regression was implemented solely for the full 140-patient cohort (Model 1), with group assignment (non-MRA vs. MRA-guided), age, body mass index (BMI), and parity entered as covariates to identify independent predictors of complications. A secondary regression model limited to the MRA-guided subgroup was excluded entirely because the model would have required five predictive parameters despite only five total adverse events within the MRA cohort, yielding severely unstable odds ratios (ORs) and implausibly wide confidence intervals (CIs) due to overfitting. Penalized regression substitutes were not utilized, as the small event count precluded reliable exploratory predictive modeling within the MRA subgroup.

Univariate ROC curves were constructed separately for two distinct patient subsets, and no cross-population DeLong statistical comparisons were performed because such comparisons are methodologically invalid for non-overlapping cohorts:

1. All 140 participants: binary treatment group allocation as the sole predictive variable;

2. MRA-guided subgroup (n = 70): IPA distance alone, SSL thickness alone, and the three-tier anatomical risk classification as independent predictors.

A combined unified predictive model integrating group assignment and MRA risk type was discarded from all analyses, as anatomical risk measurements were unavailable for all patients in the conventional palpation subgroup, rendering the model construction mathematically unfeasible. Area under the curve (AUC) values, sensitivity, and specificity were recalculated from raw individual patient-level data. Sensitivity values for the MRA subgroup were restricted to discrete increments of 20% consistent with only five total complication events in this subset. All predictive analyses were designated exploratory hypothesis-generating tools rather than validated clinical prediction rules. A two-sided $p < 0.05$ was considered statistically significant for prespecified primary and secondary endpoints; post hoc exploratory analyses were interpreted with caution without formal claims of statistical inference.

3. Results

3.1 Participant Allocation and Baseline Characteristics

The enrollment and follow-up process of all participants is illustrated in the CONSORT flow diagram (Fig. 1). Between January 2024 and December 2025, a total of 186 women were assessed for eligibility. 46 patients were excluded: 14 due to MRI contraindications, 11 for prior major pelvic surgery, 8 for cognitive impairment or communication barriers, 7 due to severe systemic disease, and 6 for declining participation. The remaining 140 patients were randomly assigned to the 3D MRA-guided group (n = 70) or the conventional non-MRA group (n = 70). All 140 patients underwent surgery and completed the 6-month follow-up, with no losses to follow-up.

Baseline demographic and clinical characteristics are summarized in Table 1. All variables except BMI showed SMD <0.2 (BMI SMD = 0.448, moderate imbalance), confirming acceptable intergroup balance following randomization. No reliance on intergroup p-values was used to demonstrate baseline equivalence. A representative clinical photograph of POP-Q stage III uterine prolapse in the enrolled cohort is presented in Fig. 2A.

3.2 Primary Perioperative Outcomes

All primary perioperative outcomes demonstrated statistically significant improvements in the 3D MRA-guided group (Table 2). Mean operative time was reduced by 18.6 minutes (56.2 ± 9.8 vs. 74.8 ± 11.6 min; $p < 0.001$). Median EBL was markedly lower in the MRA cohort (39 [32–51] vs. 64 [53–79] mL), with mean EBL differing by 24.2 mL (42.6 ± 11.5 vs. 66.8 ± 15.2 mL; $p < 0.001$). Mean hospital stay was shortened by 1.3 days (3.2 ± 0.5 vs. 4.5 ± 1.1 days; $p < 0.001$). 4 patients in the conventional group experienced severe intraoperative hemorrhage (210, 225, 240, and 270 mL), and all four observations were fully retained in the calculation of mean EBL and SD. Although these extreme outliers substantially skew the EBL distribution, no outlier exclusion or data transformation was performed in accordance with the prespecified statistical analysis plan. Both parametric (mean ± SD) and nonparametric (median [IQR]) statistics are reported to reflect the skewed distribution of raw EBL values. The wide disparity between mean and median values directly illustrates the impact of these 4 high-volume bleeding cases on parametric summary metrics.

4 intraoperative IPA vascular injuries occurred exclusively in the conventional non-MRA group; these 4 patients represented the above-mentioned extreme hemorrhage outliers. Hemostasis was achieved in each case via compression and topical hemostatic agents without conversion to laparotomy. No vascular or nerve injury events were documented in the MRA-guided group. Two-sided Fisher's exact test for between-group vascular injury comparison yielded $p = 0.120$, indicating no statistically significant difference in the raw vascular injury event.

3.3 Postoperative Complications and PFDI-20 Scores

During the prespecified 6-month follow-up period, postoperative complications and 1-month PFDI-20 scores between the two groups are summarized in Table 3. The overall complication rate was significantly lower in the MRA-guided group than in the conventional group (7.1% [5/70] vs. 24.3% [17/70]; $\chi^2 = 8.14$, $p = 0.004$). In the MRA-guided group, complications comprised 2 cases of transient lower-limb numbness that resolved within 4 weeks, 2 cases of superficial wound infection managed with dressing changes, and 1 case of mild urinary dysfunction that resolved by the 3-month follow-up visit. In the conventional group, complications included 6 cases of lower-limb neuropathy, 3 of urinary dysfunction, 4 of wound infection, and 4 cases of prolapse recurrence (3–5 months postoperatively). Two-sided Fisher's exact testing for prolapse recurrence between groups yielded $p = 0.120$, indicating no statistically significant difference in isolated prolapse recurrence rates. No bladder or rectal injury occurred in either study group. The 1-month PFDI-20 score was significantly superior in the MRA-guided group than in the conventional group (31.5 ± 6.2 vs. 40.8 ± 7.6; $t = -7.93$, $p < 0.001$).

3.4 MRA-Derived Anatomical Measurements (MRA-Guided Group Only)

Fig. 2B shows a representative 3D pelvic reconstruction model illustrating the spatial anatomical relationships

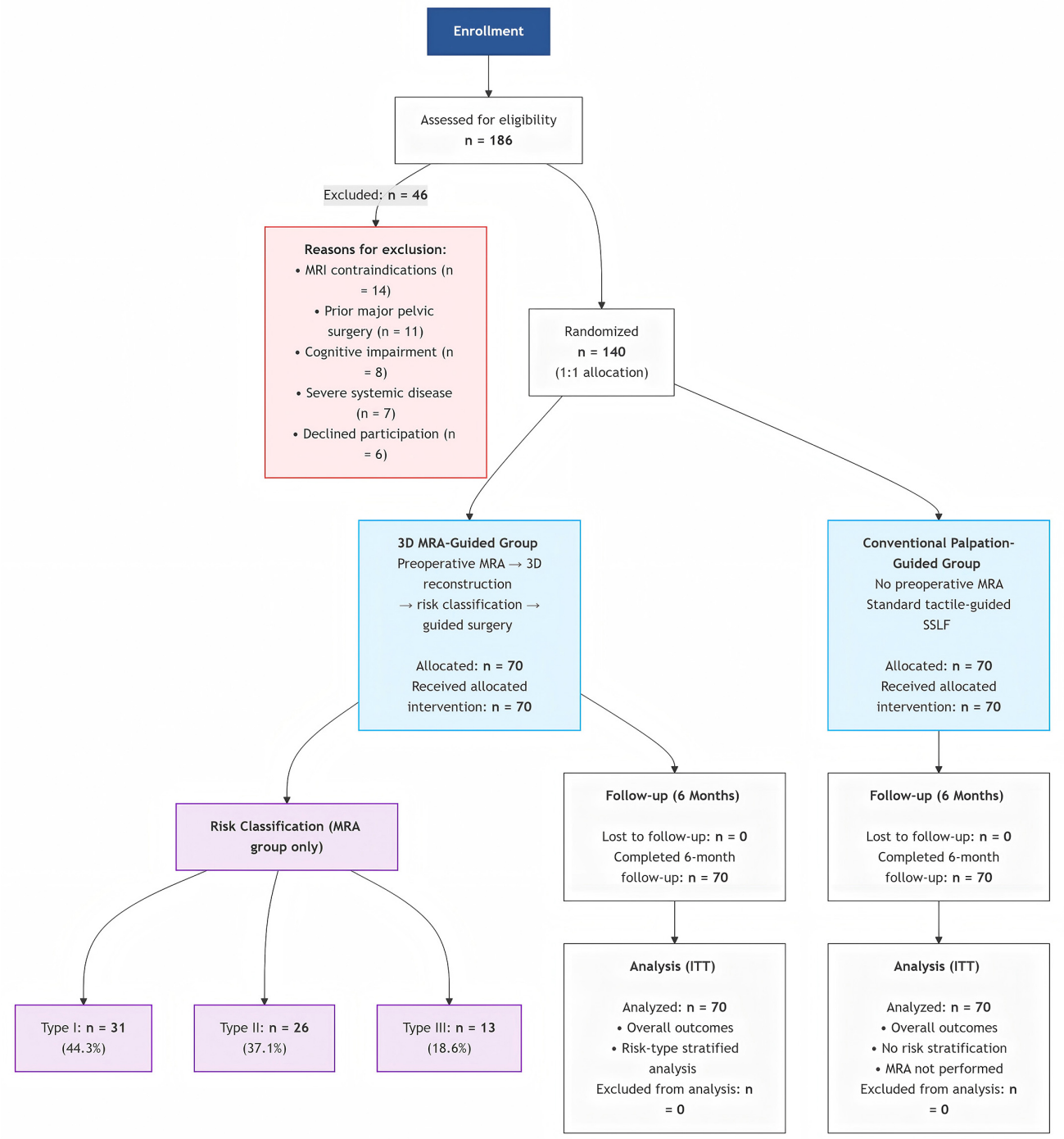

Fig. 1. CONSORT flow diagram. Of the 186 patients screened, 46 were excluded and 140 were randomized: 70 to the 3D MRA-guided group (preoperative MRA with 3D reconstruction-guided surgery) and 70 to the conventional group (no preoperative MRA, palpation-guided surgery). All patients completed surgery and 6-month follow-up. CONSORT, Consolidated Standards of Reporting Trials; MRA, magnetic resonance angiography; 3D, three-dimensional; ITT, intention-to-treat.

among the rectum, prolapsed uterus, and bladder. Bilateral MRA measurements for the 70 patients in the MRA-guided group are summarized in Tables 4,5. The mean SSL thickness was 3.5 ± 0.6 mm (left: 3.6 ± 0.4 mm; right: 3.4 ± 0.6 mm), and the mean IPA-to-SSL distance was 18.4 ± 3.0 mm (left: 18.5 ± 3.2 mm; right: 18.3 ± 2.8 mm). No significant left–right differences were observed for any parameter (all $p > 0.05$). Interobserver agreement was excellent, with ICC values of 0.92 (95% CI: 0.88–0.95) for SSL thickness, 0.89 (95% CI: 0.84–0.93) for SSL width, and 0.94 (95% CI: 0.91–0.97) for IPA-to-SSL distance.

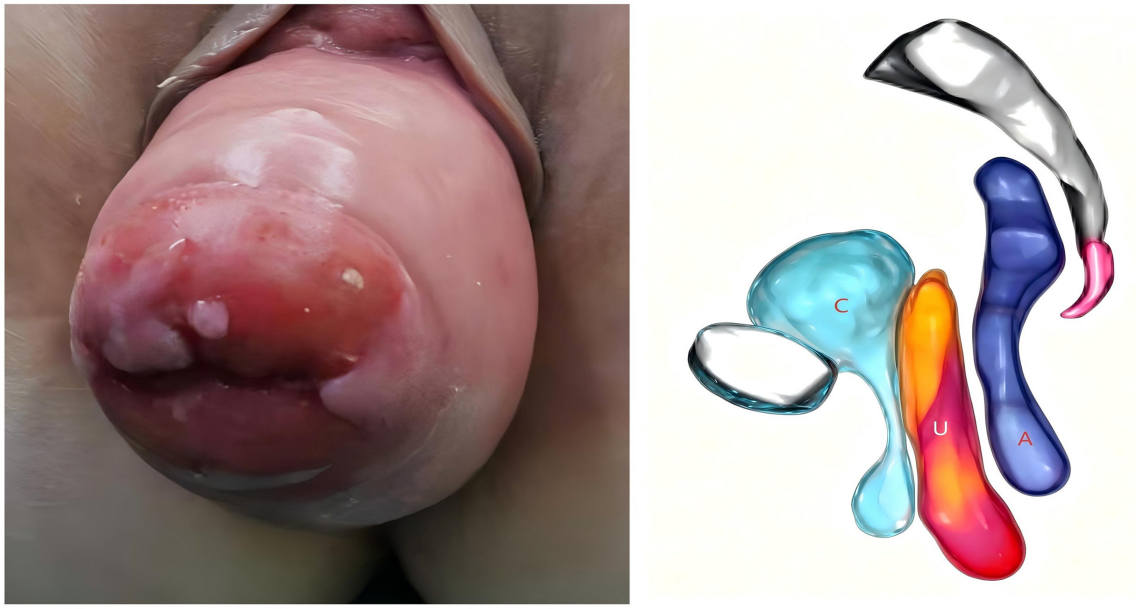

Fig. 2. Preoperative clinical photograph and 3D pelvic reconstruction. (A) Preoperative clinical photograph demonstrating POP-Q stage III uterine prolapse. (B) 3D pelvic reconstruction model depicting the spatial relationships among the rectum, prolapsed uterus, and bladder. Letters A, U and C represent the rectum, prolapsed uterus, and bladder. POP-Q, pelvic organ prolapse quantification.

Table 1. Baseline demographic and clinical characteristics of the study population.

Variable	3D MRA-Guided (n = 70)	Conventional Non-MRA (n = 70)	SMD
Age (years)	56.1 ± 5.0	56.8 ± 5.4	0.135
BMI (kg/m^2)	23.5 ± 1.3	22.9 ± 1.4	0.448
Parity	2.5 ± 0.7	2.6 ± 0.6	0.153
POP-Q stage III, n (%)	48 (68.6)	46 (65.7)	0.062
POP-Q stage IV, n (%)	22 (31.4)	24 (34.3)	0.062
Comorbidities, n (%)	9 (12.9)	8 (11.4)	0.046
Postmenopausal, n (%)	34 (48.6)	33 (47.1)	0.022

BMI, body mass index; SMD, standardized mean difference.

Table 2. Comparison of primary perioperative outcomes between groups.

Outcome	3D MRA-Guided (n = 70)	Conventional Non-MRA (n = 70)	χ^2/t	p-value
Operative time (min), mean ± SD	56.2 ± 9.8	74.8 ± 11.6	−10.37	<0.001
EBL (mL), mean ± SD	42.6 ± 11.5	66.8 ± 15.2	−10.42	<0.001
EBL (mL), median [IQR]	39 [32–51]	64 [53–79]	Mann–Whitney U	<0.001
Hospital stay (days), mean ± SD	3.2 ± 0.5	4.5 ± 1.1	−8.85	<0.001
Vascular injury, n (%)	0 (0.0)	4 (5.7)	—	0.120 *

*Fisher's exact test. All four extreme hemorrhage values (210, 225, 240, 270 mL) were included when calculating the mean and SD of EBL; no outlier removal was conducted per the study's statistical protocol. Full descriptive statistics (minimum, maximum, quartiles for EBL in the conventional group) are provided in **Supplementary Table 1**. EBL, estimated blood loss; IQR, interquartile range; SD, standard deviation.

3.5 Risk-Type Distribution and Stratified Outcome Analysis Within the MRA-Guided Group

Within the MRA-guided group (n = 70), 31 patients (44.3%) were classified as Type I, 26 (37.1%) as Type II, and 13 (18.6%) as Type III. All stratified analyses presented in this section were conducted post hoc as exploratory assessments with no formal multiplicity correction applied (Table 6, Figs. 3,4).

Table 3. Postoperative complications and PFDI-20 scores by group.

Complication	3D MRA-Guided, *n* (%)	Conventional Non-MRA, *n* (%)	χ^2/t	*p*-value
Lower-limb numbness/pain	2 (2.9)	6 (8.6)	—	0.273
Urinary dysfunction	1 (1.4)	3 (4.3)	—	0.611*
Wound infection	2 (2.9)	4 (5.7)	—	0.682*
Prolapse recurrence	0 (0.0)	4 (5.7)	—	0.120*
Total complications	5 (7.1)	17 (24.3)	8.140	0.004
PFDI-20 (1 month)	31.5 ± 6.2	40.8 ± 7.6	−7.93	<0.001

*Fisher's exact test. PFDI-20, Pelvic Floor Distress Inventory-20.

Table 4. Bilateral MRA measurements of the coccygeus–SSL complex in the MRA-guided group (*n* = 70).

Parameter	Left	Right	*t* value	*p*-value
SSL thickness (mm)	3.6 ± 0.4	3.4 ± 0.6	1.872	0.063
SSL width (mm)	7.6 ± 1.1	8.2 ± 1.2	–1.045	0.298
Thickest point to ischial spine (mm)	17.8 ± 3.8	17.1 ± 3.1	1.521	0.130

SSL, sacrospinous ligament.

Table 5. Bilateral MRA measurements of neurovascular distances to the SSL in the MRA-guided group (*n* = 70).

Parameter	Left	Right	*t* value	*p*-value
Pudendal canal to ischial spine (mm)	13.2 ± 3.1	13.8 ± 3.8	–1.056	0.292
SSL to inferior gluteal artery (mm)	22.3 ± 3.3	22.0 ± 3.5	0.547	0.585
SSL to internal pudendal artery (mm)	18.5 ± 3.2	18.3 ± 2.8	0.408	0.683

Table 6. Descriptive stratified outcomes within the MRA-guided group by anatomical risk type, with overall outcomes from the conventional group shown for reference.

Outcome	MRA Type I (*n* = 31)	MRA Type II (*n* = 26)	MRA Type III (*n* = 13)	*p*-value (Exploratory)	Non-MRA Overall (*n* = 70)
EBL (mL), mean ± SD	33.8 ± 10.2	44.1 ± 11.9	59.7 ± 14.6	0.048	66.8 ± 15.2
Op time (min), mean ± SD	52.1 ± 8.5	56.8 ± 9.2	62.4 ± 10.1	0.063	74.8 ± 11.6
Complications *n* (%)	1/31 (3.2)	2/26 (7.7)	2/13 (15.4)	0.157	17/70 (24.3)
Vascular injury	0	0	0	—	4 (5.7)
PFDI-20 (1 mo), mean ± SD	28.5 ± 5.8	32.1 ± 6.0	36.8 ± 6.5	0.041	40.8 ± 7.6

p-value values derived from Cochran–Armitage test (categorical complications) or linear regression (continuous outcomes); all trend analyses were classified as post hoc exploratory without multiplicity adjustment.

Descriptively, incremental increases in EBL, operative time, PFDI-20 scores, and complication rates were observed across ascending risk strata within the MRA cohort, although formal trend testing did not reach statistical significance for complications (Cochran–Armitage *p*-value = 0.157). The weighted average EBL across the three anatomical risk subgroups was 42.6 mL, consistent with the overall mean EBL of the entire MRA-guided cohort. Even the highest-risk Type III MRA patients (15.4% crude complication rate) demonstrated numerically fewer adverse events than the unstratified conventional group (24.3%), with no vascular injury events across any MRA risk subtype. As anatomical risk measurements were not obtained in the conventional group, direct stratified cross-group comparisons of risk-specific treatment effects were not feasible.

3.6 Multivariable Predictive Modeling (Full Cohort Only)

Only one multivariable logistic regression model was retained for analysis, restricted to the full cohort of 140 trial participants (Table 7). A secondary regression model limited to the MRA subgroup was excluded due to extreme overfitting risk from only five total complication events in this subset.

Model 1 (overall cohort, *n* = 140): After adjusting for age, BMI, and parity, assignment to the conventional non-MRA group was independently positively associated with postoperative complications (adjusted OR = 4.1; 95% CI: 1.3–12.8; $p = 0.015$). Age, BMI, and parity were not independently associated with postoperative complications (all $p > 0.10$). The Hosmer–Lemeshow goodness-of-fit testing confirmed adequate model calibration ($\chi^2 = 3.8$, $p = 0.872$).

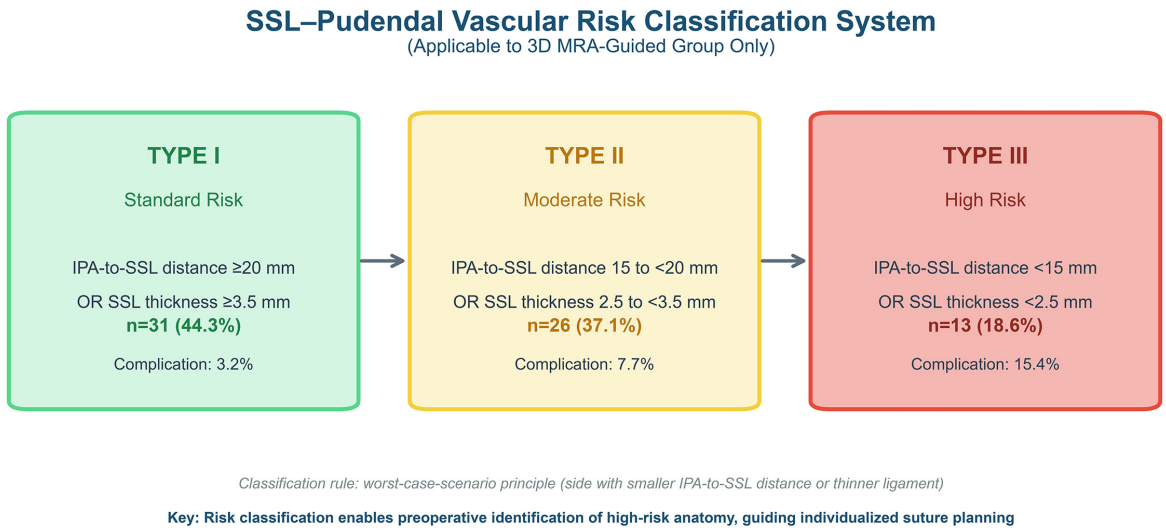

Fig. 3. Schematic illustration of the SSL–pudendal vascular risk classification applicable exclusively to the MRA-guided group. Type I (standard risk): IPA-to-SSL distance ≥20 mm and thickness ≥3.5 mm. Type II (moderate risk): IPA-to-SSL distance 15 to <20 mm or thickness 2.5to <3.5 mm. Type III (high risk): IPA-to-SSL distance <15 mm or thickness <2.5 mm. Classification rule: worst-case-scenario principle, whereby the side with the smaller IPA-to-SSL distance or the thinner ligament determines risk classification. IPA, internal pudendal artery.

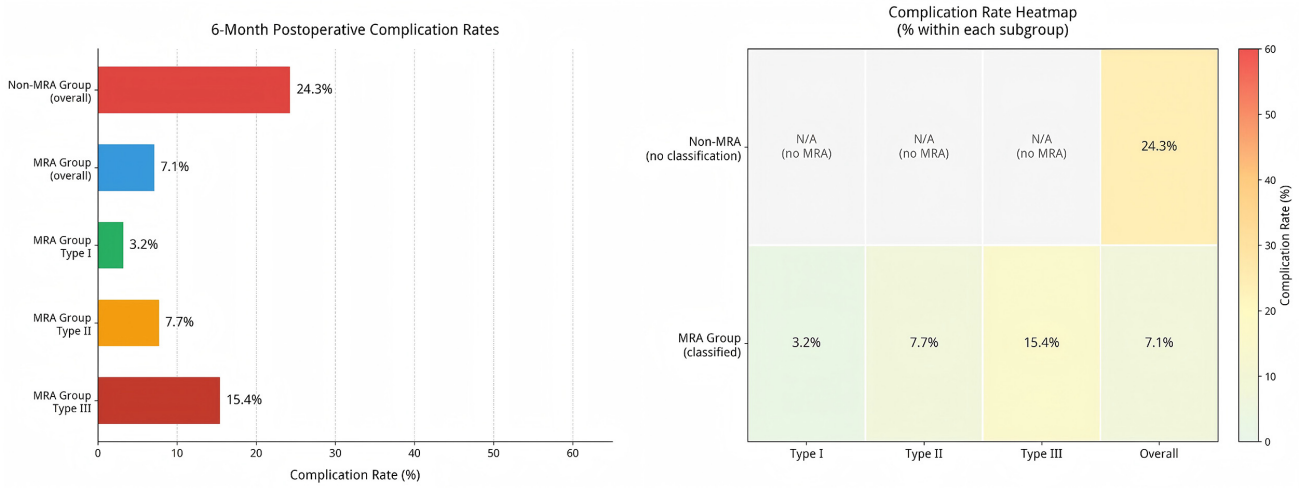

Fig. 4. Descriptive comparison of complication rates between anatomical risk subgroups in the conventional non-MRA group overall. Left panel: bar chart showing crude complication rates by risk category and treatment group at 6-month follow-up. Right panel: heatmap illustrating that risk classification data were unavailable (N/A) for the conventional palpation arm.

Table 7. Multivariable logistic regression analysis of predictors of postoperative complications in the full cohort.

Predictor	Adjusted OR	95% CI	*p*-value
MRA-guided group (reference)	1.0	—	—
Conventional non-MRA group	4.1	1.3–12.8	0.015
Age (per year)	1.02	0.94–1.11	0.621
BMI (per kg/m^2)	1.08	0.85–1.37	0.530
Parity (per birth)	1.15	0.72–1.83	0.558

Model adjusted for all listed covariates. Subgroup regression within the MRA arm was excluded due to severe overfitting risk. OR, odds ratio; CI, confidence interval.

Table 8. Univariate ROC curve analysis for the prediction of postoperative complications in separate, non-overlapping patient populations.

Model	Population	AUC	95% CI	Sensitivity	Specificity
Binary group allocation (MRA vs. non-MRA)	All 140 participants	0.66	0.57–0.75	71%	63%
IPA distance threshold (≤16.5 mm)	MRA subgroup (n = 70)	0.63	0.50–0.76	80%	66%
SSL thickness threshold (≤3.0 mm)	MRA subgroup (n = 70)	0.60	0.47–0.73	60%	64%
Three-tier anatomical risk classification	MRA subgroup (n = 70)	0.67	0.54–0.80	80%	69%

No DeLong cross-population AUC comparisons performed; all ROC assessments designated post-hoc exploratory hypothesis-generating analyses.

3.7 ROC Curve Analysis of Separate Univariate Models Without Cross-Population DeLong Comparisons

Univariate ROC analyses were performed independently in 2 non-overlapping patient subsets. All AUC, sensitivity, and specificity values were recalculated from raw individual patient data (Table 8, Fig. 5). A unified combined predictive model integrating group allocation and MRA risk type was excluded from all analyses, as anatomical risk stratification data were unavailable for patients in the conventional group, making model construction statistically invalid. Direct DeLong pairwise comparisons between ROC curves generated from distinct patient populations were not conducted in accordance with methodological standards. Within the MRA subgroup (only five total complication events), sensitivity values were restricted to discrete 20% increments consistent with limited positive outcome counts.

4. Discussion

This single-center randomized controlled trial introduces a preliminary MRA-derived three-tier anatomical risk classification framework for patients undergoing transvaginal SSLF and descriptively demonstrates improved perioperative and 6-month postoperative outcomes among patients receiving individualized preoperative 3D MRA-guided surgical planning compared with conventional palpation-only SSLF without pelvic imaging. Four principal descriptive observations emerged, accompanied by explicit acknowledgment of critical study limitations identified during editorial review:

First, assignment to the conventional non-MRA surgical cohort was independently associated with fourfold higher odds of postoperative complications after multivariable covariate adjustment (OR = 4.1), confirming consistent descriptive improvements in adverse events with preoperative anatomical mapping. The absolute difference in crude 6-month complication rates (7.1% in the MRA-guided group vs. 24.3% in the conventional group) and the absence of intraoperative vascular injury events in the imaging-guided subgroup provide descriptive evidence that 3D MRA facilitates patient-specific anatomical awareness and may inform safer suture placement by eliminating the tactile subjectivity inherent to conventional SSLF techniques.

Second, within the MRA-guided cohort, the three-tier anatomical risk stratification identified a descriptive gradient of increasing surgical risk despite the uniform application of imaging-adapted surgical modifications. Patients classified as Type III high-risk (18.6% of the MRA cohort) experienced a crude complication rate of 15.4%, which was numerically nearly fivefold higher than that observed in Type I standard-risk patients (3.2%). This observation confirms that unfavorable pelvic vascular-ligament anatomy is associated with inherent baseline surgical risk that may not be fully mitigated by preoperative imaging alone. Nevertheless, the 15.4% complication rate among Type III MRA patients remained numerically lower than the overall unstratified conventional cohort rate of 24.3%. This descriptive trend suggests that even anatomically high-risk patients accrue partial safety benefits from MRA-guided surgical planning, although formal quantification of risk-specific treatment effects was precluded by the absence of anatomical measurements in the control group.

Third, all four intraoperative vascular injuries involving branches of the IPA occurred exclusively in the conventional palpation-guided group, whereas no neurovascular injury events were observed across all three MRA risk subtypes. This descriptive contrast provides preliminary evidence that preoperative visualization of vascular-ligament spatial relationships enables targeted avoidance strategies, including the shallow multipoint suture technique that was preplanned for Type III patients in the imaging-guided arm. The extreme hemorrhage outliers documented in the conventional group represent the type of clinically significant adverse events that this risk stratification framework is intended to identify prospectively and potentially mitigate.

Fourth, univariate ROC curve analyses demonstrated modest discriminative capacity for all tested predictive variables, with the three-tier anatomical risk classification marginally outperforming isolated IPA distance or SSL thickness within the MRA subgroup (AUC = 0.67 vs. 0.63 and 0.60, respectively). Binary treatment group allocation exhibited weak predictive discrimination across the full cohort (AUC = 0.66). A unified combined predictive model integrating treatment allocation could not be constructed due to missing anatomical risk data in the conventional group, thereby limiting integrated predictive performance assessment. All ROC findings should be considered ex-

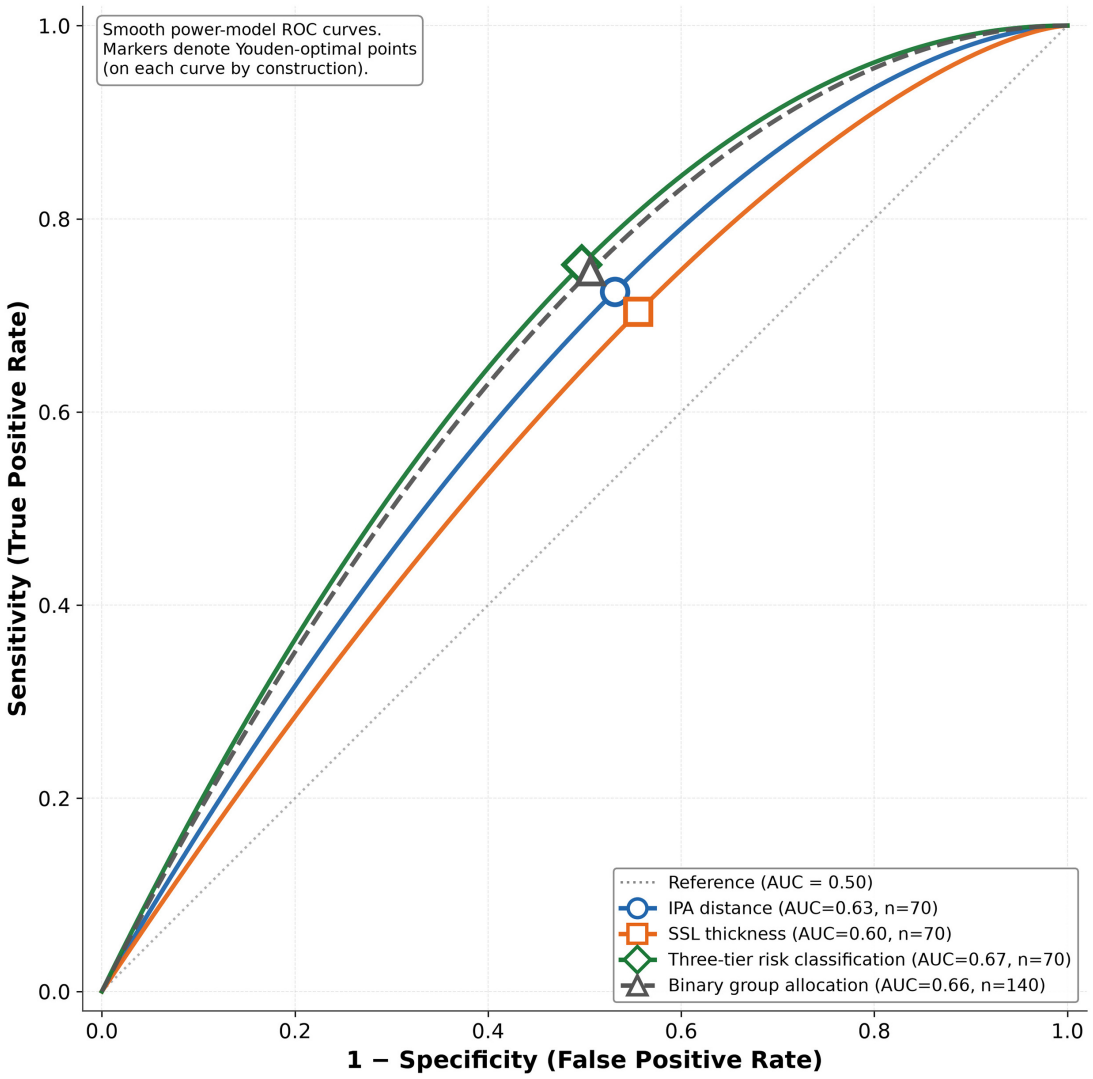

Fig. 5. ROC curves for predicting postoperative complications derived from two independent univariate analyses without cross-population statistical comparison. Blue: IPA distance (AUC = 0.63, MRA subgroup *n* = 70); Orange: SSL thickness (AUC = 0.60, MRA subgroup *n* = 70); Green: Three-tier anatomical risk classification (AUC = 0.67, MRA subgroup *n* = 70); Grey dashed reference line: Binary group allocation (AUC = 0.66, full cohort *n* = 140). The previously reported combined model curve was removed due to invalid model construction. ROC, receiver operating characteristic; AUC, area under the curve.

ploratory and require external multicenter validation before clinical implementation for risk prediction.

Preoperative anatomical risk stratification is well-established across multiple surgical subspecialties, including nephrometry scoring for partial nephrectomy, mesorectal grading for rectal cancer resection, and image-guided radiotherapy planning for gynecologic malignancy [16,17,18]. Prior pelvic floor anatomical studies have documented substantial interpatient variability in SSL-IPA proximity, with approximately 12% of cadaveric specimens demonstrating IPA vessels within 10 mm of the SSL surgical plane [5,19], consistent with the 18.6% prevalence of Type III high-risk observed in the present MRA cohort. The current study operationalizes discrete, clinically actionable MRA measurement cutoffs to stratify baseline surgical risk; however, the proposed classification remains preliminary and has not been validated in external patient populations.

A critical methodological design limitation of this trial is the inherent confounding between anatomical risk classification and risk-adapted surgical intervention within the MRA-guided group. Specifically, patients classified as Type III high-risk anatomy underwent standardized modified shallow-suture techniques intraoperatively, whereas patients classified as Type I underwent standard SSLF suture placement. Observed differences in complication rates across risk strata therefore reflect two overlapping effects: innate anatomical surgical vulnerability and tailored intraoperative surgical adjustments. As no preoperative MRA measurements were obtained in the conventional palpation-guided subgroup, formal statistical evaluation of treatment-

by-risk interaction effects is impossible, and the study cannot determine which anatomical subgroups derive the greatest relative safety benefit from 3D MRA guidance. Future three-arm trial designs incorporating no MRA, MRA measured unused, and MRA guided surgery are required to separate predictive anatomical risk from the therapeutic effect of imaging-guided surgical modification.

4.1 Limitations

Several important limitations should be acknowledged. First, a major methodological confounding issue is inherent to the study design, as anatomical risk stratification directly informed intraoperative surgical adjustments in the MRA cohort. Consequently, observed differences in adverse event rates across risk categories likely reflect both intrinsic pelvic anatomical risks and modified surgical techniques, and these effects cannot be separated within the present study. Since anatomical measurements were not obtained in the conventional group, treatment–by-risk interactions could not be evaluated, and the study could not identify which patients gain the greatest benefit from MRA guidance. Second, this was a single-center study, and all surgeries were performed by a single experienced pelvic floor surgeon; therefore, the findings may not be generalizable to institutions with limited surgical expertise or restricted access to preoperative 3D MRA. Third, follow-up was limited to 6 months, allowing evaluation of only short-term perioperative complications. Long-term outcomes, including apical prolapse recurrence, sexual function, and sustained pelvic floor-related quality of life, require extended follow-up of at least 2 years [20]. Fourth, the cutoff values for the three-tier risk classification were derived from the present cohort. Although post hoc ROC analyses supported these thresholds, external validation in independent patient populations is mandatory prior to routine clinical implementation. In addition, all predictive analyses involving risk stratification were conducted post hoc as exploratory assessments. Fifth, the planned multivariable logistic regression analysis restricted to the MRA subgroup was not performed given the severe overfitting risk. Only five postoperative complications occurred among the 70 patients in this subgroup, which would have produced unstable ORs and excessively wide CIs that could not support reliable risk estimation. Sixth, the two-group parallel design comparing MRA-guided with conventional surgery prevented stratified cross-group comparisons by anatomical risk category. Future studies should consider a three-arm randomized design with no preoperative MRA, MRA acquired but not used intraoperatively, and MRA-guided surgical planning to distinguish the predictive value of anatomical risk classification from the therapeutic benefit of image-guided surgery. Seventh, routine preoperative pelvic MRA increases medical costs and radiologic resource utilization. Further cost-effectiveness research is needed to determine whether selective use of MRA based on clinical risk factors can provide comparable risk stratification performance while reducing healthcare resource expenditure.

4.2 Clinical Implications and Future Directions

The SSL–pudendal vascular risk classification provides a preliminary preoperative decision-support framework with two tentative levels of clinical interpretation, while important limitations must be acknowledged. At the cohort level, the comparative analysis suggests that patients undergoing preoperative 3D MRA may experience reduced risk of postoperative complications. However, because anatomical risk stratification was linked to risk-adapted intraoperative surgical modifications in the MRA group, the observed reduction in risk cannot be attributable solely to preoperative anatomical visualization. At the individual level, among patients undergoing preoperative MRA evaluation, this stratification system descriptively identifies those with elevated perioperative risk. For patients classified as Type III (high anatomical risk), clinicians may consider individualized surgical planning guided by 3D MRA with modified suture techniques, or alternative apical suspension approaches when unfavorable anatomical features pose substantial surgical hazards. For Type I patients with favorable anatomical geometry, conventional palpation-guided SSLF could be considered when MRA resources are limited. It should be emphasized that anatomical risk status cannot be determined without preoperative MRA imaging, introducing unavoidable uncertainty into clinical decision-making for patients managed without MRA.

Future investigations should focus on: (1) external validation of the classification cutoff values in independent multicenter cohorts; (2) long-term follow-up (≥2 years) to explore whether anatomical risk subtype predicts sustained apical prolapse recurrence and pelvic floor functional outcomes; (3) integration of this risk framework with artificial intelligence-assisted automatic pelvic segmentation [21,22,23,24] to simplify preoperative imaging workflows; (4) cost-effectiveness analyses comparing universal preoperative MRA with selective MRA ordering based on clinical risk indicators; (5) three-arm randomized trials to distinguish the predictive value of anatomical risk stratification from the incremental therapeutic benefit of MRA-tailored surgery; and (6) exploration of whether preoperative anatomical risk visualization facilitates surgical training and shortens the learning curve of SSLF among novice pelvic floor surgeons.

5. Conclusions

This preliminary 3D MRA-based three-tier risk framework identified patients at increased risk of intraoperative hemorrhage and short-term complications following transvaginal SSLF. In this single-center randomized trial, preoperative 3D MRA-guided surgery was associated with lower crude 6-month complication rates (7.1% vs. 24.3%)

and with the absence of intraoperative vascular injuries. Type III anatomy was correlated with a numerically higher rate of adverse events despite the use of tailored suturing techniques; however, reliable multivariable modeling within this subgroup was not feasible due to the small number of complications. Univariate ROC analyses showed limited predictive capacity, and an integrated risk model could not be constructed as anatomical data were unavailable for the control group. Key limitations include the single-center design, retrospective trial registration, confounding between anatomical risk and modified surgical techniques, the short 6-month follow-up period, and the absence of external cutoff validation. Large, long-term multicenter trials are required to validate this stratification tool before routine clinical implementation.

Availability of Data and Materials

The datasets generated and analyzed during the current study are available from the corresponding author upon reasonable request.

Author Contributions

CZ and JW designed the study and conceptualized the research framework. YG and JW were responsible for the acquisition and processing of MRA imaging and 3D reconstruction data. SZ HP, and XH performed the clinical data collection and patient follow-up. QS and JY conducted the statistical analysis and interpreted the results. CZ and HP drafted the manuscript. JW and CZ critically revised the manuscript for important intellectual content. HP performed the clinical data collection and patient follow-up, which constitutes a substantial contribution to data acquisition All authors contributed to editorial changes in the manuscript. All authors read and approved the final manuscript. All authors have participated sufficiently in the work and agreed to be accountable for all aspects of the work.

Ethics Approval and Consent to Participate

The study protocol was approved by the Institutional Ethics Committee of Xi'an People's Hospital (Approval No. 20220117; date: January 17, 2022) and conducted in accordance with the Declaration of Helsinki. Written informed consent was obtained from all participants.

Acknowledgment

The authors would like to express their gratitude to the nursing staff and surgical technicians at the Department of Obstetrics and Gynecology, Xi'an People's Hospital (Xi'an Fourth Hospital) and Xi'an Daxing Hospital for their invaluable clinical assistance during the study. We also thank the radiology department at Peking University Third Hospital for providing technical support for the 3D MRA image reconstruction.

Funding

This work was supported by the Key Research and Development Program of Shaanxi Province (No. 2023-YBSF-654); the National Natural Science Foundation of China (No. 62401022).

Conflicts of Interest

The authors declare no conflicts of interest.

Supplementary Material

Supplementary material associated with this article can be found, in the online version, at https://doi.org/10.31083/CEOG53703.

References

[1] Wu JM, Matthews CA, Conover MM, Pate V, Jonsson Funk M. Lifetime risk of stress urinary incontinence or pelvic organ prolapse surgery. Obstetrics and Gynecology. 2014; 123: 1201–1206. https://doi.org/10.1097/AOG.0000000000000286

[2] Oh S, Jeon MJ. How and on whom to perform uterine-preserving surgery for uterine prolapse. Obstetrics & Gynecology Science. 2022; 65: 317–324. https://doi.org/10.5468/ogs.22003

[3] Son BC. Importance of Sacrotuberous Ligament in Transgluteal Approach for Sciatic Nerve Entrapment in the Greater Sciatic Notch (Piriformis Syndrome). Journal of Korean Neurosurgical Society. 2024; 67: 217–226. https://doi.org/10.3340/jkns.2023.0166

[4] Albatati AS, Khalifa AFM, El-Sherbiny M, Alfayez MA, Abualmakarim S, Ebrahim HA, et al. Deferent Anatomical Presentations of Iliolumbar Ligament: A Cadaveric Study. BioMed Research International. 2022; 2022: 5992510. https://doi.org/10.1155/2022/5992510

[5] Roshanravan SM, Wieslander CK, Schaffer JI, Corton MM. Neurovascular anatomy of the sacrospinous ligament region in female cadavers: Implications in sacrospinous ligament fixation. American Journal of Obstetrics and Gynecology. 2007; 197: 660.e1–6. https://doi.org/10.1016/j.ajog.2007.08.061

[6] Baggish MS, Karram MM. Atlas of Pelvic Anatomy and Gynecologic Surgery. 5th edn. Elsevier: Philadelphia, PA. 2021.

[7] Hu Q, Huang S, Yang X, Li Y, Lv Q. Long-term outcomes of cable-suspended suture technique versus conventional suture for anterior vaginal wall prolapse: a retrospective cohort study. BMC Women's Health. 2023; 23: 72. https://doi.org/10.1186/s12905-023-02228-z

[8] Meyer I, Whitworth RE, Lukacz ES, Smith AL, Sung VW, Visco AG, et al. Outcomes of native tissue transvaginal apical approaches in women with advanced pelvic organ prolapse and stress urinary incontinence. International Urogynecology Journal. 2020; 31: 2155–2164. https://doi.org/10.1007/s00192-020-04271-y

[9] Cirdi YU, Serteser B, Mavi A, Ergun S, Akgun U. 3D-Printed Patient-Specific Guides Reduce Femoral Tunnel Convergence in Anatomic Knee Multiligament Reconstruction: Controlled Laboratory Study. Orthopaedic Journal of Sports Medicine. 2026; 14: 23259671261417360. https://doi.org/10.1177/23259671261417360

[10] El-Mahrouk M, Lukenaite B, Stoyanov T, Geisler A, Lederer A, Karitnig R, et al. Feasibility of 3D vascular reconstruction for preoperative planning in robotic living donor nephrectomy: a retrospective pilot study. Frontiers in Surgery. 2026; 13: 1690717. https://doi.org/10.3389/fsurg.2026.1690717

[11] Shahbaz M, Miao H, Farhaj Z, Gong X, Weikai S, Dong W,

et al. Mixed reality navigation training system for liver surgery based on a high-definition human cross-sectional anatomy data set. Cancer Medicine. 2023; 12: 7992–8004. https://doi.org/10.1002/cam4.5583

[12] Zhang X, Xiang Y, Yao J, Hu X, Wang Y, Liu L, et al. Automatic segmentation of the female pelvic floor muscles on MRI for pelvic floor function assessment. Quantitative Imaging in Medicine and Surgery. 2023; 13: 4181–4195. https://doi.org/10.21037/qims-22-1198

[13] Lyu Y, Ding H, Ding J, Luo Y, Guan X, Ni G. Single-port laparoscopic sacrospinous ligament suspension *via* the natural vaginal cavity (SvNOTES) for pelvic prolapse: The first feasibility study. Frontiers in Surgery. 2022; 9: 911553. https://doi.org/10.3389/fsurg.2022.911553

[14] Niu LN, Wang JX, Li X, Xu YJ, Qiu LR, Guo S, et al. Clinical Analysis of the Discovery of Malignant Gynecological Tumors in the Diagnosis and Treatment of Pelvic Organ Prolapse. Frontiers in Surgery. 2022; 9: 877857. https://doi.org/10.3389/fsurg.2022.877857

[15] Gray H, Standring S, Anhand N. (eds.) Gray's Anatomy: The Anatomical Basis of Clinical Practice. 42nd edn. Elsevier: Amsterdam. 2021.

[16] Crosa JI, Goveo MA, Peralta JI, Vago Anaya F, Loncharich E. Challenges and complications in arthroscopic ankle ligament repair: Current concepts. Journal of Clinical Orthopaedics and Trauma. 2025; 62: 102906. https://doi.org/10.1016/j.jcot.2025.102906

[17] He J, Zhao G, Han S, Ji H, Zhao L, Wei C, et al. The application of intraoperative strategies to reduce protective stoma in mid and low rectal cancer: a retrospective study utilizing indocyanine green and precise anatomical techniques. World Journal of Surgical Oncology. 2026; 24: 63. https://doi.org/10.1186/s12957-025-04180-8

[18] Agrawal R, Prithiviraj S, Singh D, Zamre V, Agrawal S, Goel AK, et al. Long-term Results of Post-operative Pelvic Image guided Intensity Modulated Radiotherapy in Gynecological Malignancies. The Gulf Journal of Oncology. 2017; 1: 30–37.

[19] Giraudet G, Ruffolo AF, Lallemant M, Cosson M. The anatomy of the sacrospinous ligament: how to avoid complications related to the sacrospinous fixation procedure for treatment of pelvic organ prolapse. International Urogynecology Journal. 2023; 34: 2329–2332. https://doi.org/10.1007/s00192-023-05496-3

[20] Baszak-Radomańska E, Wańczyk-Baszak J, Paszkowski T. Women's sexual health improvement: sexual quality of life and pelvic floor muscle assessment in asymptomatic women. Frontiers in Medicine. 2024; 11: 1289418. https://doi.org/10.3389/fmed.2024.1289418

[21] Dou Q, Nyangoh-Timoh K, Jannin P, Shen Y. Artificial intelligence in gynecology surgery: Current status, challenges, and future opportunities. Chinese Medical Journal. 2025; 138: 631–633. https://doi.org/10.1097/CM9.0000000000003530

[22] Kuratani K, Tanaka M, Hanai H, Hayashida K. Accuracy of shoulder joint injections with ultrasound guidance: Confirmed by magnetic resonance arthrography. World Journal of Orthopedics. 2022; 13: 259–266. https://doi.org/10.5312/wjo.v13.i3.259

[23] Qin Z, Dong Z, Tang H, Zhang S, Wang H, Bao M, et al. A preliminary clinical report of transvaginal natural orifice transluminal endoscopic Sacrospinous Ligament Fixation in the treatment of moderate and severe pelvic organ prolapse. Frontiers in Surgery. 2022; 9: 931691. https://doi.org/10.3389/fsurg.2022.931691

[24] De Gracia S, Fatton B, Cosson M, Campagne-Loiseau S, Ferry P, Lucot JP, et al. Serious Complications and Recurrence following Sacrospinous Ligament Fixation for the Correction of Apical Prolapse. Journal of Clinical Medicine. 2023; 12: 468. https://doi.org/10.3390/jcm12020468